Prostate-derived circulating microRNAs add prognostic value to prostate cancer risk calculators

Morgan L. Zenner,[1,2] Brenna Kirkpatrick,[1,2] Trevor R. Leonardo,[3,4] Michael J. Schlicht,[1] Alejandra Cavazos Saldana,[1,2] Candice Loitz,[1,2] Klara Valyi-Nagy,[1] Mark Maienschein-Cline,[5] Peter H. Gann,[1,2] Michael Abern,[6] and Larisa Nonn,[1,2]

[1]Department of Pathology, University of Illinois at Chicago, Chicago, IL 60612, USA
[2]University of Illinois Cancer Center, Chicago, IL 60612, USA
[3]Department of Microbiology and Immunology, University of Illinois Chicago, Chicago, IL, USA
[4]Department of Periodontics, Center for Wound Healing and Tissue Regeneration, University of Illinois Chicago, Chicago, IL, USA
[4]Research Resource Core Bioinformatics, University of Illinois at Chicago, Chicago, IL 60612, USA
[5] Department of Urology, University of Illinois at Chicago, Chicago, IL 60612, USA

Correspondence: Larisa Nonn, PhD
Professor of Pathology
840 S. Wood St.
Chicago, IL 60612
312-996-0194
lnonn@uic.edu

Running title: Serum microRNAs predict prostate cancer risk

The authors have declared that no conflict of interest exists.

Abstract

Prostate cancer is the second leading cause of malignancy-related deaths among American men; however, hundreds of thousands of men live with indolent disease. Active surveillance is a safe option for men with low-risk disease. Many patients are treated with radical prostatectomy or radiation therapy, both of which have associated morbidity. Herein, we sought to identify prostate-derived microRNAs in patient sera and serum extracellular vesicles, and determine if those microRNAs added to current clinical nomograms for prostate cancer prognosis pre- and post-biopsy. Intracellular and extracellular vesicle-contained microRNAs from prostate cancer patient samples were profiled by next-generation RNA sequencing. Abundant microRNAs were included in a custom microRNA PCR panel that was queried in whole serum and serum extracellular vesicles from a diverse cohort of men diagnosed with prostate cancer. Statistical modeling showed that the levels of these circulating microRNAs significantly differed between indolent and aggressive disease and added prognostic value to pretreatment nomograms for prostate cancer disease risk. The microRNAs within the extracellular vesicles had improved prognostic value compared to the microRNAs in the whole serum. In summary, quantifying microRNAs circulating in extracellular vesicles is a clinically feasible assay that may provide additional information for assessing prostate cancer risk stratification.

Introduction

Prostate cancer (PCa) is the most diagnosed cancer and the second most common cause of death due to malignancy among men in the United States (US) (1), with one in eight men in the US being diagnosed during their lifetime (1). Because many men with PCa will die from other causes (2), a current challenge is determining which patients will develop aggressive, metastatic PCa, and which patients will have indolent, localized PCa (3). The five-year relative survival rate drops from 100% in patients with localized PCa to 32.3% in patients with metastatic disease (4), lending urgency to developing improved prognostic strategies.

PCa is diagnosed based on histological examination of a multiple-core prostate biopsy (5, 6). PCa aggressiveness is determined by the Gleason grading system (5, 7), which includes a primary and secondary grade, ranging from 3 to 5, with 3 representing cancer with moderately differentiated glands and 5 representing highly anaplastic cells (5). The sum of the Gleason grades is the Gleason score, (7), which is then classified into a Gleason Grade Group (GG) ranging from 1-5, with GG1 as the lowest grade PCa (Gleason 3+3) and GG5 as the highest grade PCa (Gleason 4+5, 5+4, or 5+5) (6, 8). The challenge with biopsies is that even with MRI guidance, they are a somewhat random sampling of the peripheral zone, which can lead to false-negative results. Thus, a low Gleason grade on biopsy tissue does not rule out the presence of a high-grade tumor that was not biopsied (9, 10).

For PCa prognosis after biopsy, urologists combine GG with the clinical stage, serum total prostate-specific antigen (PSA), PSA density, and percentage of positive biopsy cores to stratify patients into risk groups (6). These risk groups predict the risk of biochemical recurrence (BCR), which is a rise in PSA after primary treatment and is indicative of metastases. Risk group and life expectancy information are used to guide treatment recommendations in a shared decision process with the patient (6). The treatment options for localized PCa include active surveillance, radical prostatectomy (RP), radiation therapy (RT), cryotherapy, and high-intensity–focused ultrasound (6). Active surveillance is indicated for men with low-risk PCa and

involves repeat PSA testing, digital rectal exams (DRE), and biopsies (6). Compared with active surveillance, RP decreases PCa metastasis and mortality rates (11-13). Biopsy GG does not always align with GG of the RP as 30-45% of patients have upgraded and 10% have downgraded GG at RP compared with GG at biopsy (9, 10). However, both RP and RT are associated with adverse side effects such as urinary incontinence, erectile dysfunction, and proctitis (14), and thus carry their own risks. These factors contribute to the difficulties faced by patients and clinicians when making PCa treatment choices.

To aid in treatment decisions, multiple nomograms have been developed to provide personalized risk predictions at various stages of diagnosis (6, 15-18). The Prostate Biopsy Collaborative Group (PBCG) risk calculator is assessed prebiopsy to predict the likelihood of a positive biopsy (15). This nomogram, or risk calculator, considers race, age, serum PSA levels, DRE results, prior biopsy results, and family history to output a predictive percentage that an individual patient will have high-grade PCa found at biopsy (15). Following a PCa-positive biopsy, the Cancer of the Prostate Risk Assessment (CAPRA) nomogram, which uses the same clinical information as PBCG with the addition of biopsy Gleason, is used to aid in treatment decisions by predicting adverse pathology of the prostate (18, 19).

Biopsy tissue-based prognostic tests have also been developed to help better guide treatment decisions (9, 10, 20). These tests are limited because they utilize a tissue sample that may not be from the most aggressive tumor area if it is missed on biopsy. Salami et al. compared three tissue-based tests in patient-matched prostate cores across grade groups and found significant differences between patient-matched GG1 and GG4 prostate cores, indicating that transcription profiles from lower-grade biopsy cores do not capture the profiles from higher-grade cores (21).

MicroRNAs (miRs) are potentially useful blood-based biomarkers because they are highly stable in circulation (22). MiRs are small non-coding RNAs ranging in size from ~18-25 nucleotides and have been studied as PCa prognostic factors in both prostate tissues and

multiple biological fluids (23, 24). Studies from our group and others have demonstrated that miRs are promising prognostic biomarkers for PCa. Our group previously identified a 14-miR serum signature predictive of nonaggressive PCa (25). Mihelich et al. compared men with high-grade PCa (30-90% Gleason 4+5) to men with low-grade PCa (100% Gleason score 6) or benign prostate hyperplasia and determined that the miRs were predictive of indolent PCa or a cancer-free status with a negative predictive value of 100% and positive predictive value of 58.8% (25). Circulating miRs are often enclosed within extracellular vesicles (EVs) (23), a heterogeneous group of vesicles with lipid bilayer membranes (26). EVs are released from cells and have functions in normal physiology and in various disease processes (27-29). Due to the stability and functionality of miRs in EVs, they have gained substantial attention as liquid biomarkers and mediators of various cancers, including PCa (30, 31).

Herein, we sought to first identify prostate-derived miRs in EVs from patient cells and tissues and then to determine the prognostic ability of serum and serum EV miRs in a diverse cohort of 203 treatment-naïve patients with biopsy-confirmed PCa. The primary endpoint was assessing the ability of circulating miRs to add prognostic value to the current clinical standard, the CAPRA nomogram, for determining adverse pathology status at RP. The secondary endpoint involved determining if the circulating miRs added to the prognostic value of the PBCG nomogram for discriminating low-grade from high-grade PCa at biopsy.

Methods

Patient-derived prostate tissue and cell cultures

Patient prostate cells and explants were derived from patient radical prostatectomy specimens via informed consent prior to surgery as outlined by the UIC Internal Review Board-approved protocol #2006-0679. The tissue was either sliced for explant culture or dissociated for cell propagation. Human primary prostate cells were grown as previously described by our lab (32, 33). Briefly, dissociated cells were plated in two separate growth media, Prostate Cell Growth

Media (PrEBM) (Lonza, Basel, Switzerland) or MCDB105, to select and support the growth of prostate epithelial (PrE) and stromal (PrS) cells, respectively. PrE were grown on collagen-coated plates, and PrS were grown on standard tissue culture plates. PrE and PrS cell type authentication was completed by RT-qPCR using epithelial and stromal-specific markers. Epithelial-specific markers were keratin 5 (KRT5) (F: CCATATCCAGAGGAAACACTGC, R: ATCGCCACTTACCGCAAGC) and keratin 18 (KRT18) (F: CACAGTCTGCTGAGGTTGGA, R: CAAGCTGGCCTTCAGATTTC). The stromal-specific markers were vimentin (VIM) (F: CGAAAACACCCTGCAATCTT, R: TCCTGGATTTCCTCTTCGTG) and Androgen Receptor (AR) (F: CCAGGGACCATGTTTTGCC, R: CGAAGACGACAAGATGGACAA).

For explant cultures, 300 μm tissue slices were generated using a Tissue Slicer (Model MD6000, Alabama R&D, Munford, AL, USA) and cultured on titanium grids that were constantly rotated in and out of PrEBM containing 50 nM R1881.

EV isolation from cells

Prior to EV isolation, cells were washed twice with Hanks' balanced salt solution (HBSS) and cultured in EV-free medium for 48h by omitting bovine sources of EVs from the media formulation. Bovine pituitary extract was excluded from PrEBM, and MCDB105 with FBS underwent 16h ultracentrifugation at 100,000 x g to remove EVs. PrE and PrS EVs were isolated using differential ultracentrifugation. After a 48h incubation, conditioned medium was collected and centrifuged at 300 x g for 10 minutes (min) to pellet cells. The supernatant was collected again and centrifuged at 2,000 x g for 20 min to pellet dead cells. The supernatant was collected and transferred to an ultracentrifuge tube and ultracentrifuged at 10,000 x g for 30 min to pellet cell debris and larger vesicles. The supernatant was transferred to a fresh ultracentrifuge tube and ultracentrifuged at 100,000 x g for 16h to pellet EVs. The EV pellet was washed in 1X phosphate-buffered saline (PBS)(no magnesium or calcium) (Corning Inc.,

Corning, NY, USA) and ultracentrifuged for 70 min at 100,000 x g. All centrifugation and ultracentrifugation steps were performed at 4°C (34). EV pellets were resuspended in 100 µL 1X PBS and used fresh, stored at 4°C overnight, or stored long term at -80°C.

EV isolation from tissues

EVs were isolated from 2.5 mL of conditioned media from tissue slice explants using the ExoQuick-TC protocol (System Biosciences, Palo Alto, CA, USA). After a 48h incubation, conditioned media were collected from tissue slices and centrifuged at 3,000 x g for 15 min at 4°C to pellet cellular debris. The supernatant was transferred to a new tube and ExoQuick-TC was added at a 1:5 ratio (1 mL ExoQuick-TC:5 mL tissue culture media). This mixture was mixed well and incubated overnight on ice at 4°C. The mixture was then centrifuged at 3,000 x g for 10 min, and the supernatant was removed from the EV pellet. The EV pellet was resuspended in 100 µL 1X PBS (no magnesium, no calcium) or purified via a bipartite resin column according to the ExoQuick-TC ULTRA protocol. EVs were used fresh, stored at 4°C overnight, or stored long term at -80°C.

EV isolation from serum

Serum was collected in BD gold-top (serum-separator) vacutainers from PCa patients prior to treatment. Upon collection, vacutainers were flipped five times and incubated for 30 min at room temperature (RT). The vacutainers were centrifuged at 1,315 relative centrifugal force (rcf) for 10 min at 4°C. The separated serum was transferred to a 15 mL conical tube, and RNase inhibitors were added. The RNase inhibitors were 40 units/µL RNaseOUT (Life Technologies, Carlsbad, CA, USA) and 20 units/µL SUPERase-IN (Life Technologies, Carlsbad, CA, USA). Serum aliquots (500 µL) were prepared, snap-frozen in liquid nitrogen, and stored at -80°C. EVs were isolated from 500 µL serum using the ExoQuick protocol (System Biosciences, Palo Alto, CA, USA), and EV pellets were immediately stored in a liquid nitrogen tank.

Nanoparticle Tracking Analysis (NTA)

EV pellets were diluted in 1X PBS (no magnesium or calcium). The NanoSight NS300 was set according to the manufacturer's protocol (MAN0541-01-EN-00, 2017). The camera level was adjusted until all vesicles were recognized by the software, and the screen gain was set to 10. The software marks counted particles in red and undetected particles in blue. The settings were adjusted such that there were 30-80 red particles and less than 5 blue particles per screen. For each sample, three 30-second videos were captured using a 488 nm laser and a syringe pump speed of 100 (Malvern Instruments, United Kingdom). The videos were automatically analyzed using the built-in NanoSight Software NTA 3.2 (Malvern Instruments, Westborough, MA, USA) using a detection threshold of 5. For the particle concentration and size analyses, particle counts were binned in 10 nm increments. The results from the control sample (PBS) were subtracted from each sample run to determine the concentration of EVs within each 10 nm size bin.

Transmission Electron Microscopy (TEM)

The EV samples underwent negative staining for TEM observations and analysis. Approximately 10-15 µL of an EV sample in 1X PBS was deposited onto a 300-mesh Formvar/Carbon-coated copper EM grid, held tightly in forceps. After 1-2 minutes, the specimen suspension was removed via capillary action using filter paper until the grid surface was damp. One drop of 2% Uranyl acetate solution (heavy metal stain) was deposited onto the grid surface for one minute. The grid was allowed to dry again via capillary action by filter paper and then examined immediately via TEM. EV samples were examined with the JEOL JEM-1400F transmission electron microscope operating at 80 kV. Digital micrographs were acquired using an AMT NanoSprint1200-S camera and AMT software (version 7.01).

CD63 ELISA

The ExoELISA-ULTRA CD63 Kit handbook instructions were followed (System Biosciences, Palo Alto, CA, USA). Serial dilutions of the CD63 protein standard were prepared according to the manual. Serum EV pellets were diluted in 100 µL 1X Dulbecco's Phosphate-Buffered Saline (DPBS), and 45 µL was used for ELISA. The protein standard dilution series and serum EV samples were incubated for 1 h at 37°C on a microtiter plate. The samples were expelled from the plate and the wells were washed. CD63 primary antibody (1:100) was added to the wells and incubated for 1 h with shaking at RT. Secondary antibody (1:5,000) was added to the wells and incubated for 1 h with shaking at RT. The ELISA substrate was then added to the plate and incubated for 15 min with shaking. The Stop buffer was added, and the plate was immediately quantified using a spectrophotometric plate reader at 450 nm. The absorbance values of the blank wells were subtracted from the sample absorbance values. These absorbance values were then inputted into the equation generated from the standard curve to obtain the EV concentration.

Western Blot

The System Biosciences EXOAB manual was followed for serum EV western blots (System Biosciences, Palo Alto, CA, USA). EVs were isolated from 500 µL of serum using ExoQuick, as described above. The EV pellet was resuspended in 200 µL RIPA buffer with 1:100 protease/phosphatase inhibitor (Cell Signaling Technology, Danvers, MA, USA), vortexed for 15 s, and incubated at room temperature for 5 min. Protein concentration was determined using the Bradford protein assay (Bio-Rad, Hercules, CA, USA), and 20 µg was loaded per lane. Laemmli buffer 2 and β-mercaptoethanol were added to each sample and heated for 5 min at 95°C, followed by 5 min on ice. Samples were run on a 4-12% Bis-Tris electrophoresis gel (Life Technologies, Carlsbad, CA, USA) and transferred onto a polyvinylidene difluoride (PVDF)

membrane (Merck Millipore, Carrigtwohill, CO, USA). The membrane was blocked with 5% dry milk in Tris-buffered saline plus 0.05% Tween (TBST) and incubated overnight at 4°C with 1:1000 primary antibody (CD63 and CD81, rabbit anti-human, EXOAB-CD63A-1/ EXOAB-CD81A-1, System Biosciences, Palo Alto, CA, USA) in TBST. The membrane was cut prior to the addition of the primary antibody so that the antibodies were not mixed. Membranes were washed with TBST and then incubated in 1:20,000 secondary antibody (Goat Anti-Rabbit HRP) in TBST for one hour. After washing, SuperSignal West Atto Ultimate Sensitivity Chemiluminescent Substrate (Thermo Fisher Scientific, Waltham, MA, USA) was added to the membranes and visualized with the iBright 1500 (Thermo Fisher Scientific, Waltham, MA, USA).

MicroRNA RNAseq library preparation and sequencing

PrE and PrS cells were cultured in 2D on four 10-centimeter plates each. At ~70% confluency, conditioned media was collected, and EVs were isolated by differential ultracentrifugation. PrE and PrS cells were directly lysed, and RNA was collected using QIAzol (Qiagen, Germany). Tissue slices were homogenized in QIAzol using the BeadRuptor 4 (OMNI International, Bedford, NH, USA). The BeadRuptor was run twice at speed level 5 (5 ms) for 30 s for tissue homogenization. RNA was isolated from epithelial cells, stromal cells, and tissue slices using the miRNeasy Mini Kit (Qiagen, Germany) and from EVs using the Serum/Plasma miRNeasy Kit (Qiagen, Germany). MiR quantification from all samples was completed with microRNA Qubit (Thermo Fisher Scientific, Waltham, MA, USA).

MiR libraries were generated from 100 ng of cell and tissue RNA, 150 ng of cell and tissue EV RNA, and 5 µL of serum EV RNA using the QIAseq miRNA Library Kit handbook (Qiagen, Germany). Briefly, 3’ and 5’ adapters were added to miRs, miRs were reverse transcribed to cDNA, and a unique molecular index (UMI) was added to each miR. The cDNA was then cleaned prior to library amplification. Libraries underwent a cleanup protocol prior to quantification and quality control steps. Library quality control and concentrations were

determined using a High Sensitivity D1000 ScreenTape with TapeStation Analysis Software A.02.02 (Agilent Technologies, Santa Clara, CA, USA) and microRNA Qubit (Thermo Fisher Scientific, Waltham, MA, USA). Libraries (10 µM) were submitted to the Roy J. Carver Biotechnology Center at the University of Illinois at Urbana-Champaign and sequenced on a HiSeq 4000 with 100 nucleotide forward single reads.

MicroRNA differential expression analysis

Raw FASTQ sequencing reads were inputted into the GeneGlobe Data Analysis Center (Qiagen, Germany). Reads were trimmed using cutadapt (35), which removed the 3' adapter and low-quality bases. MiR sequences less than 16 base pairs (bp) and UMI sequences less than 10 bp were removed. All samples passed the initial quality control checkpoints in the GeneGlobe Data Analysis Center. Reads were then mapped to miRBase (version 22) using bowtie (36), which allows up to two mismatches. Raw counts were generated by calculating the number of UMIs mapped to each miR sequence. Downstream analyses were performed using R version 3.4.1(37).

PrE, PrS, tissue slice (TSC), PrE EV, PrS EV, and TSC EV samples were initially grouped together with Serum EV samples, and piwi-interacting RNA (piRNA) were removed. Next, miRs were filtered such that only miRs with at least five raw reads in at least 50% of all samples were retained, leaving 2114 of the original 2523 miRs. The data was then separated into the following four datasets: 1) PrE EV, PrS EV, TSC EV, Serum EV; 2) PrE EV, PrS EV, TSC EV; 3) Serum EV; and 4) PrE, PrS, TSC. For each individual dataset, a DGEList object was created in EdgeR (38, 39), normalization factors were calculated using the default trimmed mean of M-values (TMM) between each pair of samples, counts per million (CPM) function with or without log2 scaling was used to generate CPM expression levels of each miR, and files were saved. Log2 scaled CPM data were used to generate all heatmaps and principal component plots (PCA) using the heatmap3, ggplot2, and cowplot packages (40-42). Differential expression

analyses were performed using EdgeR. For each dataset, a DGEList object was created, normalization factors were calculated using TMM, and genewise statistical tests were conducted using the estimateDisp, glmQLFit, glmQLFTest, and topTags functions to identify genes differentially expressed between any of the groups within each dataset. For heatmaps, only differentially expressed genes with a statistically significant adjusted p-value ≤ 0.01 by Benjamini and Hochberg method were plotted (43, 44).

Prostate cancer patient cohort description

Serum was collected from two PCa patient cohorts; one cohort included patients on active surveillance as part of the Engaging Newly Diagnosed Men About Cancer Treatment Options (ENACT) trial (IRB protocol # 2015-1294), and the second cohort included patients who had chosen RP treatment for PCa (Prostate Cancer Blood Biorepository Resource [PCBBR], IRB protocol # 2017-0807). The inclusion criteria for the ENACT trial were patients aged 76 years or younger with a recent diagnosis of very low-, low-, or low-intermediate risk PCa. Low-intermediate criteria included serum PSA < 10 ng/mL or 10-20 ng/mL with PSA density < 0.15 ng/mL, biopsy Gleason ≤ 3+4 with ≤ 3 positive cores, and clinical stage ≤ T2c. The only inclusion criterion for the PCBBR cohort was the decision to undergo RP. Due to the differences in inclusion criteria, the ENACT cohort consisted of lower-risk PCa patients (biopsy Gleason grade groups 1-2), and the PCBBR cohort consisted of relatively higher-risk PCa patients (biopsy Gleason grade groups 1-5). Age, PSA level, self-declared race, biopsy Gleason grade group, and pathological Gleason grade group data are included for each cohort. There was some overlap between these cohorts, as 25 patients in the ENACT cohort opted for RP treatment during the study. One patient terminated their participation in the study, and their samples were removed from storage prior to use. For the ENACT patient cohort, serum was collected at least eight weeks post-biopsy and prior to RP treatment (if the patient terminated active surveillance treatment). Serum was collected at least one month after biopsy but prior to

RP treatment for the PCBBR cohort. Serum samples were immediately processed upon collection, separated into 500 µL aliquots, snap-frozen, and stored at -80°C. EVs were isolated immediately from serum and stored in liquid nitrogen.

Custom reverse-transcription quantitative polymerase chain reaction (RT-qPCR) miR panel

Five µL RNA was reverse transcribed to cDNA using the miRCURY LNA RT Kit (Qiagen, Germany). MiRs (61 plus 3 controls) were quantified on a custom PCR plate using the miRCURY LNA miR SYBR Green PCR Handbook (Qiagen, Germany). PCR was run according to the handbook instructions for 40 cycles.

Normalization and filtering of qPCR values

NormFinder normalization values were generated by Gene Globe. The normalization panel for the serum samples, as determined by NormFinder, included hsa-miR-103a-3p, hsa-miR-107, hsa-miR-24-3p, hsa-miR-30c-5p, hsa-miR-93-5p, hsa-miR-19b-3p, hsa-miR-222-3p, hsa-miR-27a-3p, hsa-miR-23a-3p, and hsa-let-7b-5p. The normalization panel for the serum EV samples, as determined by NormFinder, included hsa-miR-107, hsa-miR-24-3p, hsa-miR-30c-5p, hsa-miR-93-5p, hsa-let-7i-5p, hsa-miR-222-3p, hsa-miR-27a-3p, hsa-miR-23a-3p, hsa-miR-21-5p, and hsa-miR-27b-3p. Because each normalization factor was based on the average of 10 miRs, these miRs were included in the analysis for significance based on outcomes.

A limit of detection (LOD) of 33 was applied to the Ct values. The call rate per sample was computed as the fraction of miRs with Ct lower than the LOD, and samples with a call rate <50% were removed from the dataset. Similarly, a call rate per miR was computed for all the remaining samples, and miRs with a call rate <60% were removed. Normalized delta-Ct values were computed as the difference between the NormFinder normalization factor and the miR Ct for all miRs with Ct values lower than the LOD; miRs with Ct values equal to or greater than the

LOD were set to the minimum normalized expression over all other samples for the same miR. MiRs from serum and extracellular vesicles (EVs) were processed separately.

Statistics -Random Forest Model

Statistical analyses were completed at the UIC Research Resource Center Bioinformatics Core. The following binary outcomes were considered in preparing the models: (1) Biopsy Gleason grade group 1 (low-grade) and Gleason grade group ≥ 2 (high-grade) and (2) adverse pathology or non-adverse pathology at RP. For each binary outcome, samples with missing values were removed, and *t* tests were run for each miR using data from serum and EVs separately. MiRs with a p-value < 0.05 were retained as features in the random forest model. We also included clinical features for different models: PBCG high-grade, low-grade, and negative biopsy percentages were included independently or in combination with miRs for the prediction of Gleason grade group outcomes. CAPRA score was included independently or in combination with miRs for the prediction of adverse pathology.

For each outcome and feature dataset, we trained and tested the performance of the random forest model using the randomForest() function in the randomForest package in R (45) with default parameters. Leave-one-out cross validation was performed, predicting the outcome of each sample based on a model trained on all other samples. ROC and AUC statistics were computed based on cross validation predictions using the roc() function in the pROC package in R (46). Confidence intervals of AUC statistics were computed via bootstrapping with 500 bootstrap replicates using the ci.auc() function. P-values comparing the pairwise performance of different models were computed using the Wilcoxon signed rank test between the predicted numerical values from each model.

Study Approval

Patient specimens for this study were collected by three UIC IRB-approved protocols, one for prostate tissue/cells and two for sera, #2006-0679, #2015-1294, and #2017-0807.

Data Availability

RNA sequencing and RT-qPCR files are available at GEO Accession numbers: GSE228062, GSE228371, GPL33285. R-code is available is available at https://codeocean.com/capsule/1582037/tree.

RESULTS

Distinct cell-type specific miR expression profiles for prostate-derived cells, tissues, and EVs

The prostate is composed of multiple cell types, with a fibromuscular stroma surrounding the glandular epithelium from which cancer arises. To identify prostate-derived miRs, the miR profiles of patient-derived prostate tissues, patient-derived primary prostate epithelial cells (PrE), patient-derived primary prostate stromal cells (PrS), and their EVs were characterized by small RNA next-generation sequencing (small RNAseq) (**Figure 1A**). Ex vivo prostate tissue slice cultures (TSC) (N=4) were used as the source of whole tissue miRs, and TSC EVs were isolated from 48-hour–conditioned media with ExoQuick. Cell-derived EVs were isolated by ultracentrifugation of 48-hour–conditioned media from patient-derived PrE and PrS samples (N=4 patients). Cell type was verified by gene expression of known markers; PrE markers included keratin 5 (K5) and 18 (K18), and PrS markers included androgen receptor (AR) and vimentin (VIM) (**Supplementary Figure 1**).

EVs were characterized by Nanosight Tracking Analysis (NTA), CD63 ELISA, and transmission electron microscopy (TEM) (**Figure 1B-D**). The EVs varied in size between the samples, with PrE EVs showing one uniform peak, and PrS and TSC EVs showing more heterogeneity with multiple size peaks (**Figure 1B**). EVs were CD63-positive in all samples

(**Figure 1C**), and TEM of TSC, PrE, and PrS EVs showed sizes of 50-200 nm and a classic cup-shaped morphology (**Figure 1D**).

Small RNA libraries were created (4 TSC, 4 PrE, 4 PrS, 4 TSC EV, 4 PrE EV, 4 PrS EV) and analyzed using EdgeR (38). Principal component analysis (PCA) showed that both intracellular and EV miRs clustered by sample type (**Figures 1E-F**). Of note, PrS4 and PrS EV4 did not cluster tightly with the other three PrS samples and clustered more closely with the PrE and PrE EV samples, respectively. Additionally, one of the PrE samples clustered more tightly with the TSC samples.

Differential expression analysis in EdgeR identified common miRs and those with distinct expression in TSC, PrE, and PrS samples and EV samples, which were then visualized using heatmaps and Venn diagrams. Unbiased hierarchical clustering heatmaps of miRs showed grouping by sample type ($q \leq 0.01$, **Figure 1E-F, Supplementary Tables 1-2**), which was similar to the PCA. For Venn diagram analyses, miRs were considered "detectable" with at least 500 normalized counts per million (cpm). For intracellular miRs, there were 51 detectable miRs in common between TSC, PrE, and PrS, four miRs shared between PrE and PrS, 30 miRs shared between TSC and PrE, and seven miRs shared between TSC and PrS. There were 29 TSC-specific miRs, 22 PrE-specific miRs, and seven PrS-specific miRs (**Figure 1G and Supplementary Table 3**). For EV miRs, there were 20 detectable miRs in common between TSC EV, PrE EV, and PrS EV, no miRs shared between PrE EV and PrS EV, five miRs shared between TSC EV and PrE EV, and 43 miRs shared between TSC EV and PrS EV. There were 121 TSC EV-specific miRs, no PrE EV-specific miRs, and 22 PrS EV-specific miRs (**Figure 1G** and **Supplementary Table 4).** RT-qPCR was used to validate sample type-specific miR expression profiles observed by small RNA-seq. Hsa-let-7a-5p was robustly expressed in all sample types (PrE, PrS, TSC, and EVs) by small RNA-seq, and this was validated by RT-qPCR (**Figure 1H**). Hsa-miR-203a-3p appeared to be specific to PrE/PrE EVs and TSC/TSC EV by small RNA-seq and was confirmed by RT-qPCR (**Figure 1H**). Small RNA sequencing showed

hsa-miR-199a-5p to be specific to PrS/PrS EV and TSC/TSC EV, which was confirmed by RT-qPCR (**Figure 1H**). MiR profiling showed that the stroma and epithelium have distinct EV miR populations and that almost all stromal and epithelial EV miRs were present in the EVs from ex vivo prostate tissue slices, which contain both epithelial and stromal components.

Prostatic miRs within serum extracellular vesicles as biomarkers in prostate cancer patients

Before commencing analyses of EV miRs in serum, we characterized the serum EVs and optimized the EV isolation protocol. Visualization and quantification of single vesicles by NTA and TEM showed the serum EV size peak at 100 nm (**Figure 2A-B**). Serum EVs also expressed CD63 and CD81 but not GRP78 (intracellular protein) by western blot (**Figure 2C**). Serum miRs are known to be exceptionally stable (22), the stability of serum miRs packaged in EVs has not been well described. For a serum test to have clinical utility, the miRs must remain stable at available storage temperatures and during potential delays in EV isolation. Pooled sera were aliquoted and EVs were immediately isolated or stored at 4°C, -20°C, or -80°C for seven days. Serum EVs were isolated using ExoQuick precipitation, and CD63 levels remained unchanged after a seven-day delay in EV isolation (**Figure 2D**). The expression levels of known serum miRs remained consistent after storage at 4°C, -20°C, or -80°C for seven days (**Supplementary Figure 2).**

To identify potential biomarkers for PCa, serum EV miR expression profiles from PCa patients (N=20) were examined by small RNAseq. PCA showed no clustering by the pathological Grade Group, but only six patients were higher than GG2 (**Figure 2E**). We compared the serum EV miRs to the profiles from the TSC EVs, PrE EVs, and PrS EVs (**Figure 2F**) to identify potential prostate-derived miRs in the serum. There were 18 detectable miRs in common between serum EV, TSC EV, PrE EV, and PrS EV (**Figure 2F**). Detection of hsa-let-7a-5p and hsa-miR-199a-5p in serum EV was validated by RT-qPCR (**Figure 2G**). Hsa-miR-

203a-3p was not detected in the serum RNA-seq data, and this was validated by RT-qPCR (**Figure 2G).**

Based on the RNA-seq data and current literature, we created a custom qPCR panel to quantify 61 miRs in whole serum and serum EV samples. The miRs included in the panel were (1) the 14 miRs from the Serum miR Score (25), (2) 20 miRs that were highly expressed in prostate cell or tissue EVs and serum EVs by RNAseq analysis, and (3) 27 miRs that were consistently reported in the literature as prognostic serum biomarkers for PCa (**Table 1**). The RNA-seq miRs included were either highly expressed in all sample types or had specifically high expression in a sample subgroup (epithelial cells and epithelial EVs, for example) and in serum EVs.

Whole serum and serum EV microRNAs are add prognostic value to pre-treatment clinical nomograms

A prospective study was designed to examine the prognostic ability of post-biopsy serum miRs in UIC PCa patients (N=203) (**Figure 3** and **Table 2**). Serum was prospectively collected from two PCa patient cohorts with same-day EV isolation using ExoQuick (**Figure 3**). As the adverse pathology classification of RP resections is a major predictor of disease recurrence after RP, the primary goal of this study was to identify miRs in presurgical serum that are prognostic for RP tumor pathology. Hence, the custom miR panel was run on the serum (N=81) and serum EVs (N=62) from patients who later underwent RP. Adverse pathology is defined as Gleason Grade Group 4 or 5 and/or extraprostatic disease at RP and is a hallmark of aggressive disease that is likely to progress (47). MiRs significantly different between patients with no adverse pathology and patients with adverse pathology in serum and serum EV samples were determined and included in the random forest model analyses.

CAPRA score, a clinical post-biopsy nomogram, was used for comparison (18, 48). The outputs for CAPRA are low risk (score 0-2), intermediate risk (score 3-5), and high risk (score 6-10) (18). Random forest models showed that serum miRs and serum EV miRs added to the prognostic power of CAPRA for adverse pathology. Seven serum miRs significantly improved upon the CAPRA score AUC for adverse pathology, 0.675 (95% CI:0.547-0.799), compared to the CAPRA score alone, with an AUC of 0.516 (95% CI:0.379-0.643, p = 0.010) (**Figure 4A,C** and **Supplementary Table 5**). 19 serum EV miRs were significantly different in patients with adverse pathology and improved upon the CAPRA model (**Figure 4B,C** and **Supplementary Table 5**). Adding serum EV miRs to the CAPRA model increased the AUC to 0.739 (95% CI:0.580-0.900) (p = 0.010). Some, but not all, of the significant miRs differed between serum and serum EVs. MiRs-30a-5p and 122-5p were only significant within the serum. MiRs-26b-5p, 103a-3p, 107, 30c-5p, 222-3p, 320a, 345-5p, 191-5p, 199a-5p, 221-3p, 27b-3p, 19b-3p, 93-5p, and 301a-3p were only significant within the serum EVs. MiRs-451a, 16-5p, 363-3p, 25-3p, and let-7a-5p were predictive in both whole serum and serum EVs.

Whole serum and serum EV microRNAs are significantly differ by biopsy Gleason grade group

Prebiopsy Gleason grade group differentiation was a secondary analysis, as serum samples were collected from patients at least one month post-biopsy. All patients were treatment-naïve; therefore, this analysis was completed under the assumption that the serum and serum EV miR landscape was the same pre- and post-biopsy. PBCG, a clinically utilized prebiopsy risk calculator, was used for comparison to classify high-risk PCa or low-risk PCa by biopsy (15). Random forest models showed that serum miRs and serum EV miRs added to the prognostic power of PBCG in distinguishing between low- and high-grade PCa prebiopsy. 15 serum miRs (**Figure 5A**) and 13 serum EV miRs (**Figure 5B**) differed between patients with low-grade and high-grade PCa. PBCG combined with the significant serum miRs had an AUC of

0.705 (95% CI:0.631-0.783) compared to PBCG risk alone (AUC of 0.600, 95% CI:0.521-0.686) in patients with low-grade and high-grade PCa (p = 0.164) (**Figures 5C and Supplementary Table 6**). PBCG combined with the 13 significant serum EV miRs had an AUC of 0.695 (95% CI:0.589-0.792) compared to PBCG risk alone, which had an AUC of 0.600 (95% CI:0.521-0.686) in patients with low-grade and high-grade PCa (p = 0.080) (**Figure 5C and Supplementary Table 6**). Although there were serum and serum EV miRs that were significantly different in patients with low-grade and high-grade PCa at biopsy, the miRs combined with PBCG did not reach a statistically significant difference in AUCs compared with PBCG alone.

Discussion

In this study, we report miR profiling of patient-derived prostate cells and tissues and the extracellular vesicles released from these samples. We further compared these prostate-derived miRs with those present in the serum EVs of patients with PCa. These findings led to the development of a miR panel with prognostic value for aggressive PCa using serum collected after prostate biopsy. We determined that miRs within whole serum and serum EVs added prognostic value to the CAPRA nomogram for adverse pathology and that serum EV miRs were more prognostic than whole serum miRs.

The primary clinical outcome of this study was to determine the ability of serum and serum EV miRs to add to the prognostic value of the presurgical CAPRA nomogram for determining the risk of aggressive disease after surgery. In our study cohort of 203 patients with PCa, 81 underwent RP. Pretreatment serum and serum EV miRs added to the prognostic value of the CAPRA nomogram for the adverse pathology outcome. These new findings improve upon our prior study (25) in which the predictive miRs in the “Serum miR Score” had unanimously increased expression in patients with low-grade PCa and only provided additional predictive information to patients with low-risk PCa. In this current study, serum and serum EV miRs were

significantly different in patients with AP, indicating their potential to provide clinical information to patients with both low- and high-risk PCa before making treatment decisions. Additionally, the relative expression levels of the significantly different miRs in this new panel were both higher and lower in patients with AP, compared to all 14 miRs having higher expression in low-risk PCa in our prior study (25). A strength of this new study is that we included a racially diverse patient cohort and a full range of Gleason grade groups as opposed to the previous study cohort of only white men and no intermediate-risk patients.

The secondary clinical outcome of this study was to determine the ability of circulating miRs to add prognostic value to a current prebiopsy nomogram, PBCG, which could move the miR-based clinical test earlier in the diagnostic pipeline, potentially reducing biopsies in low-risk patients. One limitation is that the serum samples were collected at least one month post-biopsy, so this analysis was completed assuming that the composition of circulating miRs was the same pre- and post-biopsy. In our study cohort, both serum and serum EV miRs significantly differed in patients with low- versus high-grade PCa; however, they only trended towards adding to the prognostic ability of PBCG ($p=0.08$). As previously discussed, there is inherent noise in the Gleason grade of prostate biopsies given that thorough sampling of the tumors is not possible. Thus, larger cohorts with prebiopsy serum and post-RP pathology are needed to test biomarkers in this space.

Considerable overlap occurred in the significant miRs between serum and serum EV sample types. Some overlap in miRs was expected because serum EVs are a component of whole serum. Additionally, there was an overlap of prognostic miRs in this study compared to the miRs included in the prognostic “Serum miR Score” from our previous study (25). Two of the 14 miRs were prognostic for AP in both serum and serum EVs (hsa-let-7a-5p and hsa-miR-451a). In the serum EV model, five additional miRs that were significant for AP overlapped with those included in the Serum miR Score. This demonstrates the reproducibility of serum miRs over multiple platforms and cohorts. Therefore, this study provides evidence that circulating

serum EVs have both overlapping and unique prognostic miRs compared to circulating miRs in whole serum and may add additional prognostic information for PCa.

Our initial characterization of prostate-derived miRs by RNA-seq revealed new expression patterns for several miRs. Given the regulatory role of miRs in cell fate (49), it was unsurprising that the miR profiles of patient-derived prostate samples showed clustering based on cell type (stromal versus epithelial) and sample type (cell versus whole tissue slices). Kumar et al. previously identified prostate stromal- and epithelial-specific miRs using microdissection of prostate tissue (50). Both studies identified that miR-141 (miR-141-3p and miR-141-5p in our dataset) was epithelial-specific and that miR-143-3p was highly expressed in stromal samples. We newly identified the miR-199 family as predominantly stromal-specific, which has not been previously reported in the prostate. The miR-199 family has been shown to have low expression in prostate tumors (51, 52). With the new knowledge that miR-199 is predominantly expressed in the prostate stroma, these reported changes in miR-199a expression in PCa compared to benign prostate tissue may be due to low stromal cells in areas of tumor compared to benign (53).

MiRs in EVs were similarly clustered by sample type with interpatient heterogeneity, and multiple miRs were determined to be specific to prostate epithelial or stromal EVs. MiR localization and secretion within EVs has been well-documented in various cell types (54). Cargo sorting into EVs was initially thought to be a random process that allowed cells to dispel molecular waste (29). However, multiple studies have determined that the sorting process is highly selective, with the secreted EV miRs remaining functional after being transferred to another cell (54, 55). In our study, robust intracellular cell type-specific miRs did not always result in high EV miRs. Of the 107 robustly expressed epithelial intracellular miRs (> 500 cpm), only 24 were also highly expressed in epithelial EVs. However, there were only 25 miRs with greater than 500 cpm in the epithelial EV sample group; therefore, there was high concordance

between the prostate epithelial cells miRs and the miRs within the EVs released from the cells (96% overlap with epithelial cells). For the stromal compartment, 50 of the 69 robustly expressed stromal miRs overlapped with stromal EV miRs with greater than 500 cpm. Again, there was a high degree of overlap between stromal cells and EVs released from these cells, as there were 85 total highly expressed miRs in the stromal EV sample group (58.8% overlap with stromal cells). These findings support the selective packaging of miRs into EVs, as not all intracellular miRs were found in EVs and not all EV miRs were highly expressed intracellularly (56). These datasets and differential expression analyses have yielded many unexplored findings regarding miR expression within the prostate and EVs released from the prostate.

Several prostate-derived miRs were also highly detectable in the circulation of patients with PCa. Isolation of serum EVs was rigorously optimized, as there have been mixed reports of serum miR stability and limited reports of serum EV miR stability in the literature. Others have previously demonstrated the stability of serum/plasma miRs after one day at room temperature, after freeze-thaw cycles, and after years of frozen storage (22, 57, 58). However, miR levels decrease after long-term storage at 4°C (57, 59), suggesting that processing should be expedited if possible. These findings demonstrate that serum EV miRs remain stable for up to one week of delayed processing at temperatures accessible to most laboratories (4, -20, and -80°C), which increases the feasibility of a clinical test.

It is important to discuss the normalization methods used for miR expression quantitation from EV and serum datasets. Currently, there are no standardized normalization methods for miRs across sample types, with even fewer reports regarding EV miRs. For the tissue and cell-based EV NGS data, we used the Trimmed Mean of M method as a function within edgeR, as this was the same method used for the cell and tissue miR data. We tested how different groupings would affect the data after normalization, so we normalized the tissue and cell-based EV samples both separately and as a larger group with the tissue and cell samples. Differential

expression results were very similar in both sets of data analysis. For the serum and serum EV prognostic miR analyses, we used the NormFinder normalization method within the GeneGlobe platform. The other normalization options within GeneGlobe included global normalization and geNorm. We chose not to use global normalization due to the potential bias of having lower or higher levels of overall miRs between patients. For our serum analysis, there were 10 miRs in the normalization panels, as determined by both geNorm and NormFinder, with seven of the miRs being consistent in both panels. This degree of overlap between normalization methods was consistent with other studies (60). In our serum EV analysis, there were 10 miRs in both the geNorm and NormFinder normalization panels, with only one consistent miR between the two panels.

This study was limited by the number of patients who chose to undergo RP treatment and, therefore, the number of samples available for prognostic analysis and model configuration. Of 203 patients, only 81 underwent RP treatment. As our patient cohort was smaller than anticipated, we did not use training and testing subgroups for prognostic model generation. However, we used random forest modeling, which allows for the inclusion of all samples in the model creation due to the bagging feature. Given this limitation, these findings would need to be validated in a prospective cohort of patients with PCa.

Considering the high rates of Gleason grade group discordance between biopsy and RP, the addition of serum/serum EV miR quantitation could be used to guide patient decisions to undergo or forgo radical prostatectomy. With more accurate pretreatment risk stratification, patients with low-risk disease may have more confidence in active surveillance protocols and avoid overtreatment, whereas high-risk patients could be appropriately treated with more aggressive measures. Future studies should assess the clinical significance of these prognostic tests and how they affect treatment recommendations and patient decisions (61).

AUTHOR CONTRIBUTIONS

M.L.Z and L.N. conceptualized the study, secured funding, analyzed data and wrote the manuscript. M.L.Z, B.K., M.J.S., A.C.S, and C.L. conducted experiments. T.R.L and M.M.C did informatic and statistical analyses. K.V.N. and M.A. secured patient samples and consent forms. P.H.G. edited manuscript and provided patient sera.

ACKNOWLEDGMENTS

We thank the patient participants who donated their specimens for this research. Blood samples were acquired with the assistance of Dr. Ruben Sauer and Ms. Patrice King-Lee. BioRender was used to prepare Figure 1A. UIC Research Resource Center Cores, Transmission Electron Microscopy Core, and Genomics Core assisted with data collection.

FUNDING STATEMENT

This research was funded by the Department of Defense Prostate Cancer Research Program W81XWH-16-1-0382 (L.N), Ruth L. Kirschstein NRSA for Individual Predoctoral MD/PhD Degree Fellowship (NIH/NCI F30 CA243197) (M.L.Z), and the CCTS Pre-doctoral Education for Clinical and Translational Scientists (PECTS) Fellowship (M.L.Z).

CONFLICT OF INTEREST DECLARATION

The authors declare that they have no affiliations with or involvement in any organization or entity with any financial interest in the subject matter or materials discussed in this manuscript.

FIGURE LEGENDS

Figure 1. Characterization of prostate-derived extracellular vesicles and microRNA profiles of patient-derived prostate samples. A) Flow chart of PCa patient-derived samples included for small RNA NGS profiling (4 tissue slice explants (TSC), 4 epithelial cell cultures (PrE), 4 stromal cell cultures (PrS), and 4 EV samples from each sample type (TSC EV, PrE EV, and PrS EV). **B)** Nanoparticle particle tracking analysis of two PrE EV samples, two PrS EV samples, and one TSC EV sample. **C)** CD63 ELISA of PrE-, PrS-, and TSC-derived EVs. (N = 3 PrE, 3 PrS, 2 TSC; Error bars show SEM). **D)** Transmission electron microscopy (TEM) images of EVs derived from PrE, PrS, and TSC (size bars = 100 nm). **E, F)** PCA plots and unbiased hierarchical clustering of the miR profiles of (**E**) Patient-derived prostate epithelial cells, stromal cells, and tissue slice explants and (**F**) EVs isolated from patient-derived prostate epithelial cells, stromal cells, and tissue slice explants (N = 4 per sample type). Heatmaps show differentially expressed miRs with an adjusted p-value ≤ 0.01 using the Benjamini-Hochberg method. **G)** Venn diagram representation of TMM-normalized miRs with > 500 counts per million (cpm) within each sample type. **H)** RT-qPCR validation of cell/EV-specific miRs as determined by NGS miR profiles (N = 2 replicates per sample, Error bars = SD, ND = not detected).

Figure 2. Characterization of patient-derived pretreatment serum extracellular vesicles and their microRNA profiles. A) Nanoparticle tracking analysis of N = 2 patient-derived serum EV samples. **B)** Transmission electron microscopy image of patient-derived serum EVs (size bar = 100 nm). **C)** Western blot of EV-specific markers (CD63 and CD81) and intracellular protein control (GRP78) of two patient-derived serum EV samples and one patient-derived stromal cell control. **D)** CD63 ELISA of patient-derived serum EV samples stored at 4, -20, and -80°C for 1 and 7 days. (N = 3 samples per day, error bars = SD). **E)** PCA plot of the miR profiles of patient-derived pretreatment serum EVs (N = 20 patients). Data are grouped by pathological Gleason Grade group (Pathological GG). **F)** Venn diagram representation of TMM-normalized miRs with > 500 counts per million (cpm) within EVs isolated from patient-derived serum, epithelial cells, stromal cells, and tissue slice explants. **G)** RT-qPCR validation of serum EV miRs as determined by NGS miR profiles (N = 2 replicates per sample, Error bars = SD, ND = not detected).

Figure 3. Patient cohort and study design. Study design flow chart for determining serum and serum EV miRs that are predictive of prostate cancer outcomes.

Figure 4. Circulating serum and serum EV microRNAs add pretreatment predictive value to the CAPRA nomogram for prostate cancer risk. A) Violin plot of serum miRs and **B)** serum EV miRs that are predictive of adverse pathology (AP). The lines on the violin plots represent the mean and first and third quartiles. Significant miRs had a p-value < 0.05. **C)** Significant serum and serum EV miRs were included with the CAPRA score in random forest models to predict AP. The area under the curve (AUC) is reported for CAPRA alone (black), CAPRA + serum miRs (red), and CAPRA + serum EV miRs (blue).

Figure 5. Circulating serum and serum EV microRNAs add prebiopsy predictive value to the PBCG nomogram for prostate cancer risk. A) Violin plot of serum miRs and B) serum EV miRs that are predictive of low-grade and high-grade PCa. Patients stratified in biopsy Gleason grade group 1 were considered low-grade; patients with biopsy Gleason grade group 2 or higher were considered high-grade. The lines on the violin plots represent the mean and first and third quartiles. Significant miRs had a p-value < 0.05.**C)** Significant serum and serum EV miRs were included with the PBCG risk in random forest models to predict low-grade and high-grade PCa. The area under the curve (AUC) is reported for PBCG alone (black), PBCG + serum miRs (red), and PBCG + serum EV miRs (blue).

REFERENCES

1. Siegel RL, Miller KD, Fuchs HE, and Jemal A. Cancer statistics, 2022. *CA: a cancer journal for clinicians.* 2022;72(1):7-33.
2. Bell KJ, Del Mar C, Wright G, Dickinson J, and Glasziou P. Prevalence of incidental prostate cancer: A systematic review of autopsy studies. *International journal of cancer.* 2015;137(7):1749-57.
3. Grossman DC, Curry SJ, Owens DK, Bibbins-Domingo K, Caughey AB, Davidson KW, et al. Screening for Prostate Cancer: US Preventive Services Task Force Recommendation Statement. *Jama.* 2018;319(18):1901-13.
4. . Surveillance Research Program, National Cancer Institute.
5. Gleason DF, and Mellinger GT. Prediction of prognosis for prostatic adenocarcinoma by combined histological grading and clinical staging. *The Journal of urology.* 1974;111(1):58-64.
6. Mohler JL, Antonarakis ES, Armstrong AJ, D'Amico AV, Davis BJ, Dorff T, et al. Prostate Cancer, Version 2.2019, NCCN Clinical Practice Guidelines in Oncology. *Journal of the National Comprehensive Cancer Network : JNCCN.* 2019;17(5):479-505.
7. Epstein JI, Egevad L, Amin MB, Delahunt B, Srigley JR, and Humphrey PA. The 2014 International Society of Urological Pathology (ISUP) Consensus Conference on Gleason Grading of Prostatic Carcinoma: Definition of Grading Patterns and Proposal for a New Grading System. *The American journal of surgical pathology.* 2016;40(2):244-52.
8. Epstein JI, Zelefsky MJ, Sjoberg DD, Nelson JB, Egevad L, Magi-Galluzzi C, et al. A Contemporary Prostate Cancer Grading System: A Validated Alternative to the Gleason Score. *European urology.* 2016;69(3):428-35.
9. Ooi K, and Samali R. Discrepancies in Gleason scoring of prostate biopsies and radical prostatectomy specimens and the effects of multiple needle biopsies on scoring accuracy. A regional experience in Tamworth, Australia. *ANZ journal of surgery.* 2007;77(5):336-8.
10. Quintana L, Ward A, Gerrin SJ, Genega EM, Rosen S, Sanda MG, et al. Gleason Misclassification Rate Is Independent of Number of Biopsy Cores in Systematic Biopsy. *Urology.* 2016;91:143-9.
11. Aas K, Dorothea Fosså S, Åge Myklebust T, Møller B, Kvåle R, Vlatkovic L, et al. Increased curative treatment is associated with decreased prostate cancer-specific and overall mortality in senior adults with high-risk prostate cancer; results from a national registry-based cohort study. *Cancer medicine.* 2020;9(18):6646-57.
12. Lei JH, Liu LR, Wei Q, Yan SB, Song TR, Lin FS, et al. Systematic review and meta-analysis of the survival outcomes of first-line treatment options in high-risk prostate cancer. *Scientific reports.* 2015;5:7713.
13. Hamdy FC, Donovan JL, Lane JA, Mason M, Metcalfe C, Holding P, et al. 10-Year Outcomes after Monitoring, Surgery, or Radiotherapy for Localized Prostate Cancer. *The New England journal of medicine.* 2016;375(15):1415-24.
14. Sanda MG, Dunn RL, Michalski J, Sandler HM, Northouse L, Hembroff L, et al. Quality of life and satisfaction with outcome among prostate-cancer survivors. *The New England journal of medicine.* 2008;358(12):1250-61.
15. Ankerst DP, Straubinger J, Selig K, Guerrios L, De Hoedt A, Hernandez J, et al. A Contemporary Prostate Biopsy Risk Calculator Based on Multiple Heterogeneous Cohorts. *European urology.* 2018;74(2):197-203.
16. Kattan M, Eastham J, and Wheeler T. Counseling men with prostate cancer: a nomogram for predicting the presence of small, moderately differentiated, confined tumors. *The Journal of urology.* 2003;170:1792-7.

17. Ondracek R, Kattan M, and Murekeyisoni C. Validation of the Kattan nomogram for prostate cancer recurrence after radical prostatectomy. *Journal of the National Comprehensive Cancer Network : JNCCN.* 2016;14:1395-401.
18. Cooperberg MR, Pasta DJ, Elkin EP, Litwin MS, Latini DM, Du Chane J, et al. The University of California, San Francisco Cancer of the Prostate Risk Assessment score: a straightforward and reliable preoperative predictor of disease recurrence after radical prostatectomy. *The Journal of urology.* 2005;173(6):1938-42.
19. Cooperberg MR, Hilton JF, and Carroll PR. The CAPRA-S score: A straightforward tool for improved prediction of outcomes after radical prostatectomy. *Cancer.* 2011;117(22):5039-46.
20. Cucchiara V, Cooperberg MR, Dall'Era M, Lin DW, Montorsi F, Schalken JA, et al. Genomic Markers in Prostate Cancer Decision Making. *European urology.* 2018;73(4):572-82.
21. Salami SS, Hovelson DH, Kaplan JB, Mathieu R, Udager AM, Curci NE, et al. Transcriptomic heterogeneity in multifocal prostate cancer. *JCI insight.* 2018;3(21).
22. Mitchell PS, Parkin RK, Kroh EM, Fritz BR, Wyman SK, Pogosova-Agadjanyan EL, et al. Circulating microRNAs as stable blood-based markers for cancer detection. *Proceedings of the National Academy of Sciences of the United States of America.* 2008;105(30):10513-8.
23. Cozar JM, Robles-Fernandez I, Rodriguez-Martinez A, Puche-Sanz I, Vazquez-Alonso F, Lorente JA, et al. The role of miRNAs as biomarkers in prostate cancer. *Mutation research.* 2019;781:165-74.
24. Ghafouri-Fard S, Shoorei H, and Taheri M. Role of microRNAs in the development, prognosis and therapeutic response of patients with prostate cancer. *Gene.* 2020;759:144995.
25. Mihelich BL, Maranville JC, Nolley R, Peehl DM, and Nonn L. Elevated serum microRNA levels associate with absence of high-grade prostate cancer in a retrospective cohort. *PloS one.* 2015;10(4):e0124245.
26. van Niel G, D'Angelo G, and Raposo G. Shedding light on the cell biology of extracellular vesicles. *Nature reviews Molecular cell biology.* 2018;19(4):213-28.
27. Aalberts M, Stout TA, and Stoorvogel W. Prostasomes: extracellular vesicles from the prostate. *Reproduction (Cambridge, England).* 2014;147(1):R1-14.
28. Linxweiler J, and Junker K. Extracellular vesicles in urological malignancies: an update. *Nature reviews Urology.* 2020;17(1):11-27.
29. Yuana Y, Sturk A, and Nieuwland R. Extracellular vesicles in physiological and pathological conditions. *Blood reviews.* 2013;27(1):31-9.
30. Wang J, Ni J, Beretov J, Thompson J, Graham P, and Li Y. Exosomal microRNAs as liquid biopsy biomarkers in prostate cancer. *Critical reviews in oncology/hematology.* 2020;145:102860.
31. Saber SH, Ali HEA, Gaballa R, Gaballah M, Ali HI, Zerfaoui M, et al. Exosomes are the Driving Force in Preparing the Soil for the Metastatic Seeds: Lessons from the Prostate Cancer. *Cells.* 2020;9(3).
32. McCray T, Pacheco JV, Loitz CC, Garcia J, Baumann B, Schlicht MJ, et al. Vitamin D sufficiency enhances differentiation of patient-derived prostate epithelial organoids. *iScience.* 2021;24(1):101974.
33. Richards Z, McCray T, Marsili J, Zenner ML, Manlucu JT, Garcia J, et al. Prostate Stroma Increases the Viability and Maintains the Branching Phenotype of Human Prostate Organoids. *iScience.* 2019;12:304-17.
34. Théry C, Amigorena S, Raposo G, and Clayton A. Isolation and characterization of exosomes from cell culture supernatants and biological fluids. *Current protocols in cell biology.* 2006;Chapter 3:Unit 3.22.

35. Martin M. Cutadapt removes adapter sequences from high-throughput sequencing reads. *EMBnetjournal.* 2011;17(1):10-2.
36. Langmead B, Trapnell C, Pop M, and Salzberg SL. Ultrafast and memory-efficient alignment of short DNA sequences to the human genome. *Genome biology.* 2021;10(25).
37. Team RC. Vienna, Austria: R Foundation for Statistical Computing; 2017.
38. Robinson MD, McCarthy DJ, and Smyth GK. edgeR: a Bioconductor package for differential expression analysis of digital gene expression data. *Bioinformatics (Oxford, England).* 2010;26(1):139-40.
39. McCarthy DJ, Chen Y, and Smyth GK. Differential expression analysis of multifactor RNA-Seq experiments with respect to biological variation. *Nucleic acids research.* 2012;40(10):4288-97.
40. Shilin Zhao LY, Yan Guo, Quanhu Sheng, Yu Shyr. *An Improved Heatmap Package*. CRAN; 2021:An improved heatmap package. Completely compatible with the original R function 'heatmap', and provides more powerful and convenient features.
41. Wickham H. *ggplot2.* New York: Springer New York.
42. Wilke CO. CRAN; 2020.
43. Sun W, Reich BJ, Cai TT, Guindani M, and Schwartzman A. False Discovery Control in Large-Scale Spatial Multiple Testing. *Journal of the Royal Statistical Society Series B, Statistical methodology.* 2015;77(1):59-83.
44. Benjamini Y, Hochberg, Y. Controlling the False Discovery Rate: a Practical and Powerful Approach to Multiple Testing. *Journal of the Royal Statistical Society Series B (Methodological).* 1995;57(1):289-300.
45. Liaw AW, M. Classification and Regression by randomForest. *R News.* 2002;2(3):18-22.
46. Robin X, Turck N, Hainard A, Tiberti N, Lisacek F, Sanchez JC, et al. pROC: an open-source package for R and S+ to analyze and compare ROC curves. *BMC bioinformatics.* 2011;12:77.
47. Kozminski MA, Tomlins S, Cole A, Singhal U, Lu L, Skolarus TA, et al. Standardizing the definition of adverse pathology for lower risk men undergoing radical prostatectomy. *Urologic oncology.* 2016;34(9):415.e1-6.
48. Cooperberg MR, Broering JM, and Carroll PR. Risk assessment for prostate cancer metastasis and mortality at the time of diagnosis. *Journal of the National Cancer Institute.* 2009;101(12):878-87.
49. Park CY, Choi YS, and McManus MT. Analysis of microRNA knockouts in mice. *Human molecular genetics.* 2010;19(R2):R169-75.
50. Kumar B, Rosenberg AZ, Choi SM, Fox-Talbot K, De Marzo AM, Nonn L, et al. Cell-type specific expression of oncogenic and tumor suppressive microRNAs in the human prostate and prostate cancer. *Scientific reports.* 2018;8(1):7189.
51. Zhong J, Huang R, Su Z, Zhang M, Xu M, Gong J, et al. Downregulation of miR-199a-5p promotes prostate adeno-carcinoma progression through loss of its inhibition of HIF-1α. *Oncotarget.* 2017;8(48):83523-38.
52. Chen L, Cao H, and Feng Y. MiR-199a suppresses prostate cancer paclitaxel resistance by targeting YES1. *World journal of urology.* 2018;36(3):357-65.
53. Boufaied N, Takhar M, Nash C, Erho N, Bismar TA, Davicioni E, et al. Development of a predictive model for stromal content in prostate cancer samples to improve signature performance. *The Journal of pathology.* 2019;249(4):411-24.
54. Melo SA, Sugimoto H, O'Connell JT, Kato N, Villanueva A, Vidal A, et al. Cancer exosomes perform cell-independent microRNA biogenesis and promote tumorigenesis. *Cancer cell.* 2014;26(5):707-21.
55. Janas T, Janas MM, Sapoń K, and Janas T. Mechanisms of RNA loading into exosomes. *FEBS letters.* 2015;589(13):1391-8.

56. Liu XM, Ma L, and Schekman R. Selective sorting of microRNAs into exosomes by phase-separated YBX1 condensates. *eLife.* 2021;10.
57. Ge Q, Zhou Y, Lu J, Bai Y, Xie X, and Lu Z. miRNA in plasma exosome is stable under different storage conditions. *Molecules (Basel, Switzerland).* 2014;19(2):1568-75.
58. Matias-Garcia PR, Wilson R, Mussack V, Reischl E, Waldenberger M, Gieger C, et al. Impact of long-term storage and freeze-thawing on eight circulating microRNAs in plasma samples. *PloS one.* 2020;15(1):e0227648.
59. Yamada A, Cox MA, Gaffney KA, Moreland A, Boland CR, and Goel A. Technical factors involved in the measurement of circulating microRNA biomarkers for the detection of colorectal neoplasia. *PloS one.* 2014;9(11):e112481.
60. Kok MG, Halliani A, Moerland PD, Meijers JC, Creemers EE, and Pinto-Sietsma SJ. Normalization panels for the reliable quantification of circulating microRNAs by RT-qPCR. *FASEB journal : official publication of the Federation of American Societies for Experimental Biology.* 2015;29(9):3853-62.
61. Murphy AB, Abern MR, Liu L, Wang H, Hollowell CMP, Sharifi R, et al. Impact of a Genomic Test on Treatment Decision in a Predominantly African American Population With Favorable-Risk Prostate Cancer: A Randomized Trial. *Journal of clinical oncology : official journal of the American Society of Clinical Oncology.* 2021;39(15):1660-70.
62. Bhagirath D, Yang TL, Bucay N, Sekhon K, Majid S, Shahryari V, et al. microRNA-1246 Is an Exosomal Biomarker for Aggressive Prostate Cancer. *Cancer research.* 2018;78(7):1833-44.
63. Brase JC, Johannes M, Schlomm T, Fälth M, Haese A, Steuber T, et al. Circulating miRNAs are correlated with tumor progression in prostate cancer. *International journal of cancer.* 2011;128(3):608-16.
64. Bryant RJ, Pawlowski T, Catto JW, Marsden G, Vessella RL, Rhees B, et al. Changes in circulating microRNA levels associated with prostate cancer. *British journal of cancer.* 2012;106(4):768-74.
65. Cheng HH, Mitchell PS, Kroh EM, Dowell AE, Chéry L, Siddiqui J, et al. Circulating microRNA profiling identifies a subset of metastatic prostate cancer patients with evidence of cancer-associated hypoxia. *PloS one.* 2013;8(7):e69239.
66. Nguyen HC, Xie W, Yang M, Hsieh CL, Drouin S, Lee GS, et al. Expression differences of circulating microRNAs in metastatic castration resistant prostate cancer and low-risk, localized prostate cancer. *The Prostate.* 2013;73(4):346-54.
67. Selth LA, Townley S, Gillis JL, Ochnik AM, Murti K, Macfarlane RJ, et al. Discovery of circulating microRNAs associated with human prostate cancer using a mouse model of disease. *International journal of cancer.* 2012;131(3):652-61.
68. Selth LA, Townley SL, Bert AG, Stricker PD, Sutherland PD, Horvath LG, et al. Circulating microRNAs predict biochemical recurrence in prostate cancer patients. *British journal of cancer.* 2013;109(3):641-50.
69. Porzycki P, Ciszkowicz E, Semik M, and Tyrka M. Combination of three miRNA (miR-141, miR-21, and miR-375) as potential diagnostic tool for prostate cancer recognition. *International urology and nephrology.* 2018;50(9):1619-26.
70. Guo X, Han T, Hu P, Guo X, Zhu C, Wang Y, et al. Five microRNAs in serum as potential biomarkers for prostate cancer risk assessment and therapeutic intervention. *International urology and nephrology.* 2018;50(12):2193-200.
71. Li Z, Ma YY, Wang J, Zeng XF, Li R, Kang W, et al. Exosomal microRNA-141 is upregulated in the serum of prostate cancer patients. *OncoTargets and therapy.* 2016;9:139-48.
72. Mao Z, Ji A, Yang K, He W, Hu Y, Zhang Q, et al. Diagnostic performance of PCA3 and hK2 in combination with serum PSA for prostate cancer. *Medicine.* 2018;97(42):e12806.

73. Zhang HL, Qin XJ, Cao DL, Zhu Y, Yao XD, Zhang SL, et al. An elevated serum miR-141 level in patients with bone-metastatic prostate cancer is correlated with more bone lesions. *Asian journal of andrology.* 2013;15(2):231-5.
74. Lodes MJ, Caraballo M, Suciu D, Munro S, Kumar A, and Anderson B. Detection of cancer with serum miRNAs on an oligonucleotide microarray. *PloS one.* 2009;4(7):e6229.
75. Zidan HE, Abdul-Maksoud RS, Elsayed WSH, and Desoky EAM. Diagnostic and prognostic value of serum miR-15a and miR-16-1 expression among egyptian patients with prostate cancer. *IUBMB life.* 2018;70(5):437-44.
76. Cochetti G, Poli G, Guelfi G, Boni A, Egidi MG, and Mearini E. Different levels of serum microRNAs in prostate cancer and benign prostatic hyperplasia: evaluation of potential diagnostic and prognostic role. *OncoTargets and therapy.* 2016;9:7545-53.
77. Wang SY, Shiboski S, Belair CD, Cooperberg MR, Simko JP, Stoppler H, et al. miR-19, miR-345, miR-519c-5p serum levels predict adverse pathology in prostate cancer patients eligible for active surveillance. *PloS one.* 2014;9(6):e98597.
78. Tinay I, Tan M, Gui B, Werner L, Kibel AS, and Jia L. Functional roles and potential clinical application of miRNA-345-5p in prostate cancer. *The Prostate.* 2018;78(12):927-37.
79. Haldrup C, Kosaka N, Ochiya T, Borre M, Høyer S, Orntoft TF, et al. Profiling of circulating microRNAs for prostate cancer biomarker discovery. *Drug delivery and translational research.* 2014;4(1):19-30.
80. Wa Q, Huang S, Pan J, Tang Y, He S, Fu X, et al. miR-204-5p Represses Bone Metastasis via Inactivating NF-κB Signaling in Prostate Cancer. *Molecular therapy Nucleic acids.* 2019;18:567-79.
81. Qu Y, and Huang W. Effects of microRNA210 on the diagnosis and treatment of prostate cancer. *Molecular medicine reports.* 2018;18(2):1740-4.
82. Fang Y, Qiu J, Jiang ZB, Xu SR, Zhou ZH, and He RL. Increased serum levels of miR-214 in patients with PCa with bone metastasis may serve as a potential biomarker by targeting PTEN. *Oncology letters.* 2019;17(1):398-405.
83. Singh PK, Preus L, Hu Q, Yan L, Long MD, Morrison CD, et al. Serum microRNA expression patterns that predict early treatment failure in prostate cancer patients. *Oncotarget.* 2014;5(3):824-40.
84. Lyu J, Zhao L, Wang F, Ji J, Cao Z, Xu H, et al. Discovery and Validation of Serum MicroRNAs as Early Diagnostic Biomarkers for Prostate Cancer in Chinese Population. *BioMed research international.* 2019;2019:9306803.
85. Gao W, Hong Z, Huang H, Zhu A, Lin S, Cheng C, et al. miR-27a in serum acts as biomarker for prostate cancer detection and promotes cell proliferation by targeting Sprouty2. *Oncology letters.* 2018;16(4):5291-8.
86. Kolluru V, Chandrasekaran B, Tyagi A, Dervishi A, Ankem M, Yan X, et al. miR-301a expression: Diagnostic and prognostic marker for prostate cancer. *Urologic oncology.* 2018;36(11):503.e9-.e15.
87. Lieb V, Weigelt K, Scheinost L, Fischer K, Greither T, Marcou M, et al. Serum levels of miR-320 family members are associated with clinical parameters and diagnosis in prostate cancer patients. *Oncotarget.* 2018;9(12):10402-16.
88. Wach S, Al-Janabi O, Weigelt K, Fischer K, Greither T, Marcou M, et al. The combined serum levels of miR-375 and urokinase plasminogen activator receptor are suggested as diagnostic and prognostic biomarkers in prostate cancer. *International journal of cancer.* 2015;137(6):1406-16.
89. Mahn R, Heukamp LC, Rogenhofer S, von Ruecker A, Müller SC, and Ellinger J. Circulating microRNAs (miRNA) in serum of patients with prostate cancer. *Urology.* 2011;77(5):1265.e9-16.

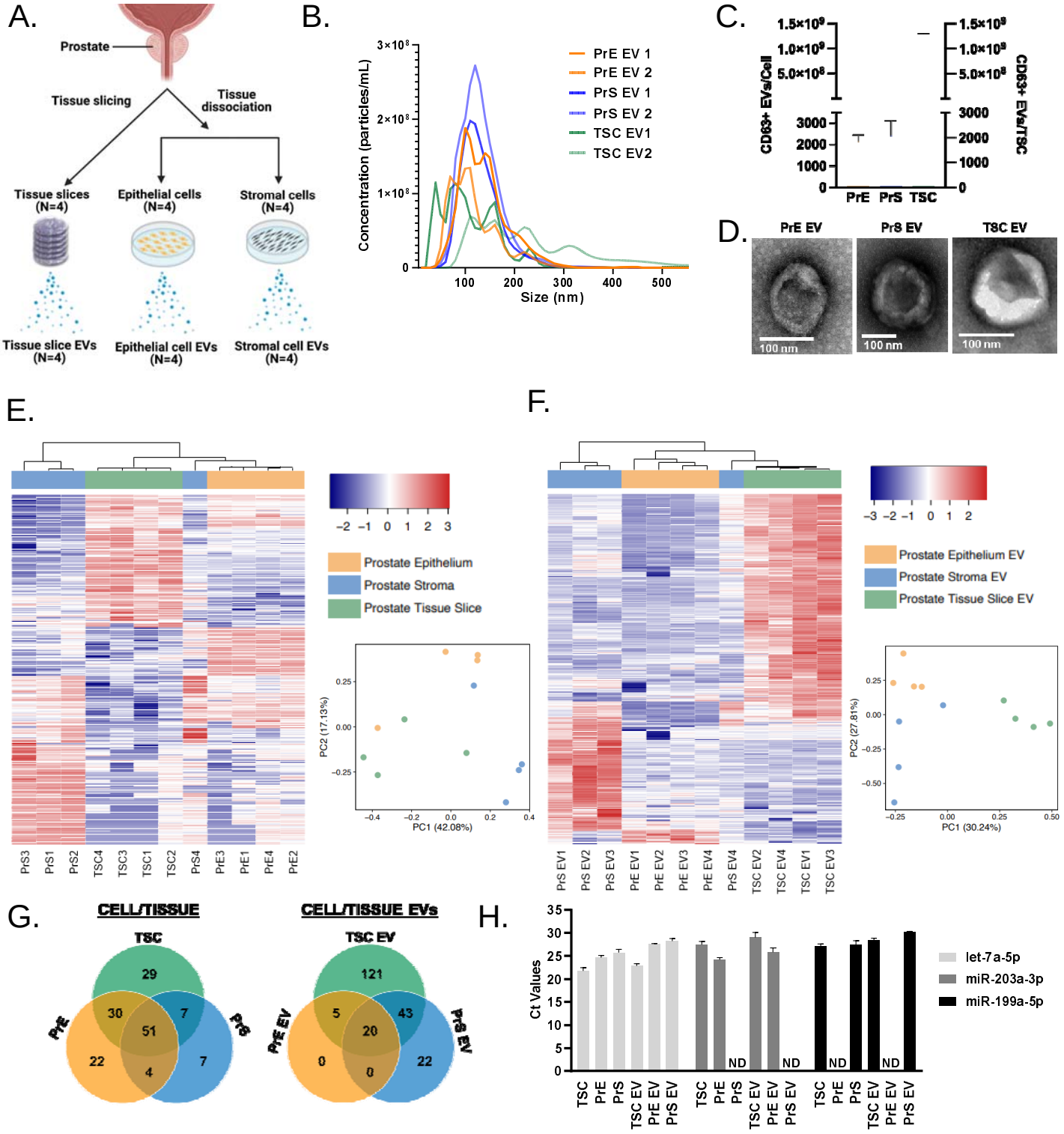
A.
Prostate
Tissue slicing
Tissue dissociation
Tissue slices (N=4)
Epithelial cells (N=4)
Stromal cells (N=4)
Tissue slice EVs (N=4)
Epithelial cell EVs (N=4)
Stromal cell EVs (N=4)
B.
Concentration (particles/mL)
Size (nm)
PrE EV 1
PrE EV 2
PrS EV 1
PrS EV 2
TSC EV1
TSC EV2
C.
CD63+ EVs/Cell
CD63+ EVs/TSC
PrE
PrS
TSC
D.
PrE EV
PrS EV
TSC EV
100 nm
E.
Prostate Epithelium
Prostate Stroma
Prostate Tissue Slice
PC1 (42.08%)
PC2 (17.13%)
PrS3 PrS1 PrS2 TSC4 TSC3 TSC1 TSC2 PrS4 PrE3 PrE1 PrE4 PrE2
F.
Prostate Epithelium EV
Prostate Stroma EV
Prostate Tissue Slice EV
PC1 (30.24%)
PC2 (27.81%)
PrS EV1 PrS EV2 PrS EV3 PrE EV1 PrE EV2 PrE EV3 PrE EV4 PrS EV4 TSC EV2 TSC EV4 TSC EV1 TSC EV3
G.
CELL/TISSUE
TSC
PrE
PrS
29
30
7
51
22
4
7
CELL/TISSUE EVs
TSC EV
PrE EV
PrS EV
121
5
43
20
0
0
22
H.
Ct Values
let-7a-5p
miR-203a-3p
miR-199a-5p
ND
TSC PrE PrS TSC EV PrE EV PrS EV

Figure 1

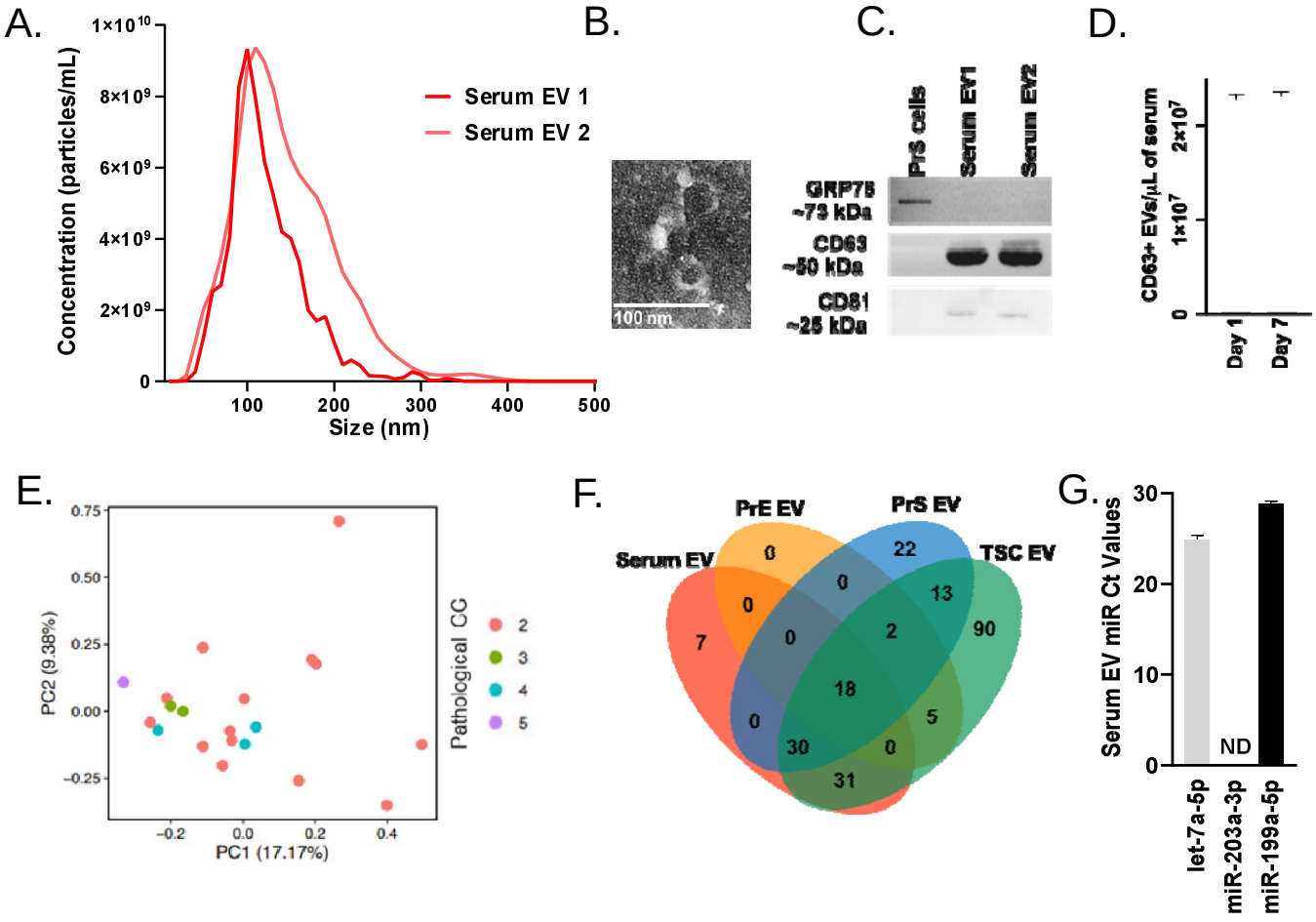
A.
Concentration (particles/mL)
Size (nm)
Serum EV 1
Serum EV 2
B.
100 nm
C.
PrS cells
Serum EV1
Serum EV2
GRP75
~73 kDa
CD63
~50 kDa
CD81
~25 kDa
D.
CD63+ EVs/µL of serum
Day 1
Day 7
E.
PC2 (9.38%)
PC1 (17.17%)
Pathological CC
F.
Serum EV
PrE EV
PrS EV
TSC EV
G.
Serum EV miR Ct Values
ND
let-7a-5p
miR-203a-3p
miR-199a-5p

Figure 2

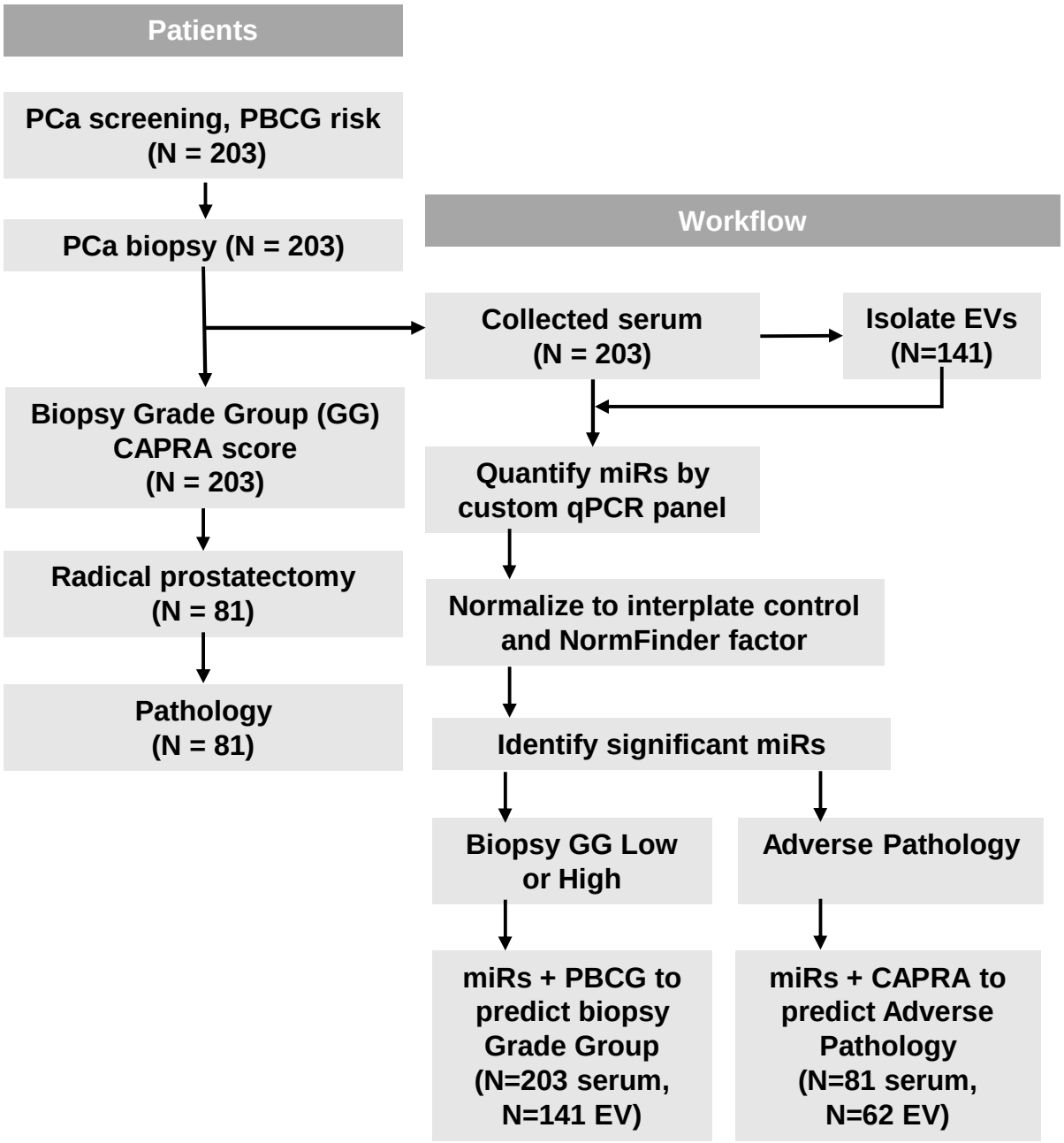
Patients
PCa screening, PBCG risk (N = 203)
PCa biopsy (N = 203)
Biopsy Grade Group (GG) CAPRA score (N = 203)
Radical prostatectomy (N = 81)
Pathology (N = 81)
Workflow
Collected serum (N = 203)
Isolate EVs (N=141)
Quantify miRs by custom qPCR panel
Normalize to interplate control and NormFinder factor
Identify significant miRs
Biopsy GG Low or High
Adverse Pathology
miRs + PBCG to predict biopsy Grade Group (N=203 serum, N=141 EV)
miRs + CAPRA to predict Adverse Pathology (N=81 serum, N=62 EV)

Figure 3

A.

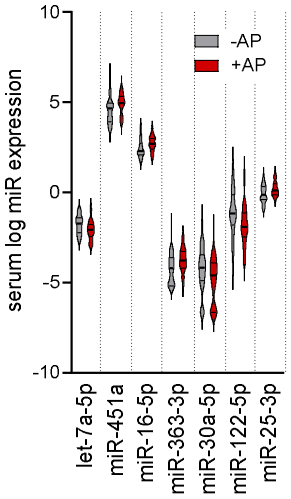
serum log miR expression
10
5
0
-5
-10
-AP
+AP
let-7a-5p
miR-451a
miR-16-5p
miR-363-3p
miR-30a-5p
miR-122-5p
miR-25-3p

B.

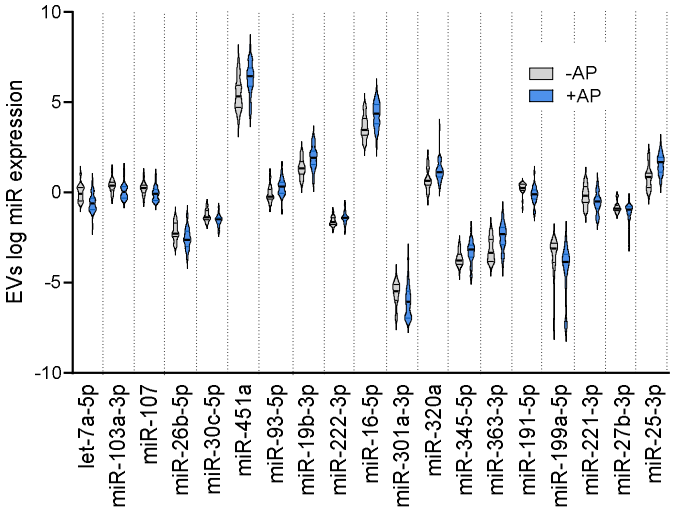
EVs log miR expression
10
5
0
-5
-10
-AP
+AP
let-7a-5p
miR-103a-3p
miR-107
miR-26b-5p
miR-30c-5p
miR-451a
miR-93-5p
miR-19b-3p
miR-222-3p
miR-16-5p
miR-301a-3p
miR-320a
miR-345-5p
miR-363-3p
miR-191-5p
miR-199a-5p
miR-221-3p
miR-27b-3p
miR-25-3p

C.

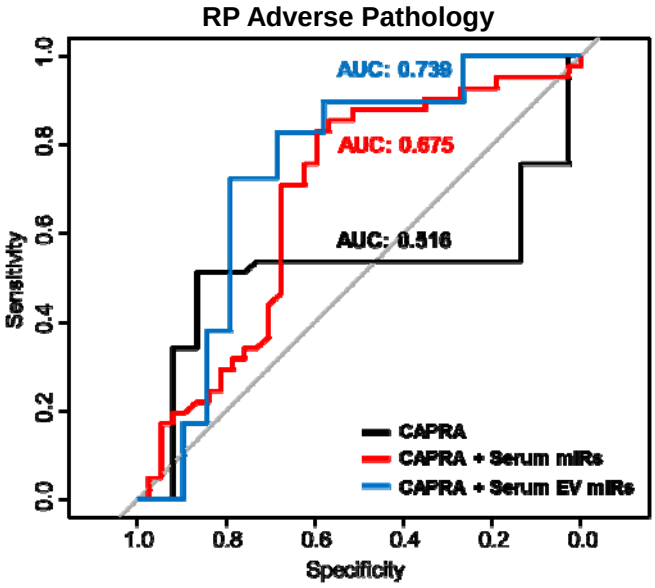
RP Adverse Pathology
AUC: 0.739
AUC: 0.675
AUC: 0.516
CAPRA
CAPRA + Serum miRs
CAPRA + Serum EV miRs
Sensitivity
Specificity
1.0
0.8
0.6
0.4
0.2
0.0

Figure 4

A.

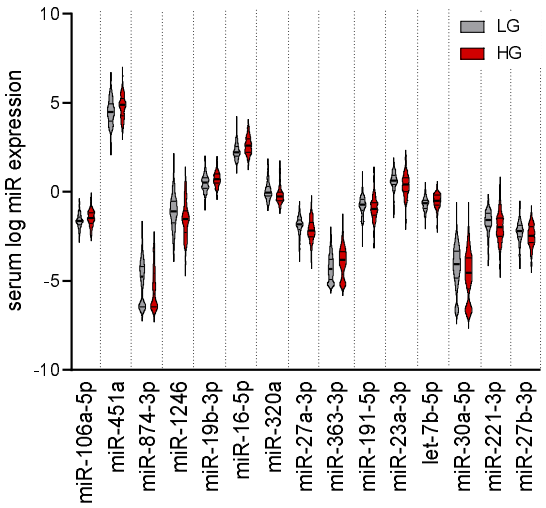
serum log miR expression
10
5
0
-5
-10
LG
HG
miR-106a-5p
miR-451a
miR-874-3p
miR-1246
miR-19b-3p
miR-16-5p
miR-320a
miR-27a-3p
miR-363-3p
miR-191-5p
miR-23a-3p
let-7b-5p
miR-30a-5p
miR-221-3p
miR-27b-3p

B.

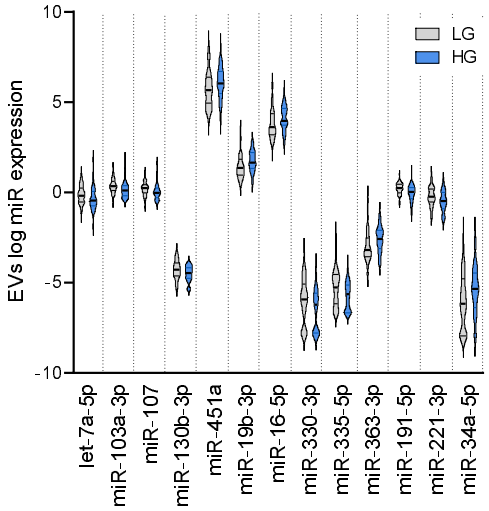
EVs log miR expression
10
5
0
-5
-10
LG
HG
let-7a-5p
miR-103a-3p
miR-107
miR-130b-3p
miR-451a
miR-19b-3p
miR-16-5p
miR-330-3p
miR-335-5p
miR-363-3p
miR-191-5p
miR-221-3p
miR-34a-5p

C.

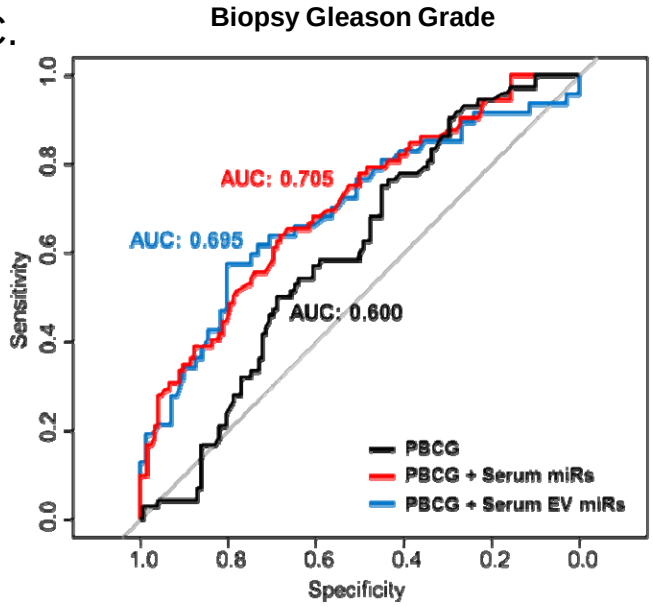
Biopsy Gleason Grade
Sensitivity
Specificity
1.0
0.8
0.6
0.4
0.2
0.0
AUC: 0.705
AUC: 0.695
AUC: 0.600
PBCG
PBCG + Serum miRs
PBCG + Serum EV miRs

Figure 5

Table 1. Custom microRNA RT-qPCR panel.

Serum miR Score (25)	**New prostate NGS Data**	**Literature search (Citation)**
hsa-let-7a-5p	hsa-let-7b-5p	hsa-miR-1246 (62)
hsa-miR-100-5p	hsa-miR-122-5p	hsa-miR-141-3p (22, 63-73)
hsa-miR-103a-3p	hsa-miR-125b-5p	hsa-miR-146b-3p (68)
hsa-miR-106a-5p	hsa-miR-143-3p	hsa-miR-16-5p (74, 75)
hsa-miR-107	hsa-miR-148a-3p	hsa-miR-18b-5p (76)
hsa-miR-130b-3p	hsa-miR-155-5p	hsa-miR-19b-3p (77)
hsa-miR-146a-5p	hsa-miR-191-5p	hsa-miR-193a-3p (78)
hsa-miR-223-3p	hsa-miR-199a-3p	hsa-miR-194-5p (68)
hsa-miR-24-3p	hsa-miR-199a-5p	hsa-miR-200a-3p (65, 79)
hsa-miR-26b-5p	hsa-miR-21-5p	hsa-miR-200b-3p (63)
hsa-miR-30c-5p	hsa-miR-218-5p	hsa-miR-204-5p (80)
hsa-miR-451a	hsa-miR-221-3p	hsa-miR-210-3p (65, 79, 81)
hsa-miR-874-3p	hsa-miR-23a-3p	hsa-miR-214-3p (82)
hsa-miR-93-5p	hsa-miR-25-3p	hsa-miR-222-3p (83)
	hsa-miR-27b-3p	hsa-miR-27a-3p (84, 85)
	hsa-miR-29a-3p	hsa-miR-301a-3p (86)
	hsa-miR-30a-5p	hsa-miR-320a (87)
	hsa-miR-31-5p	hsa-miR-330-3p (78)
	hsa-miR-34a-5p	hsa-miR-335-5p (78)
	hsa-miR-374a-5p	hsa-miR-345-5p (77)
		hsa-miR-363-3p (76)
		hsa-miR-375 (63-67, 69, 79, 88)
		hsa-miR-518e-5p (77)
		hsa-miR-574-3p (64, 74)
		hsa-miR-708-5p (79)
		hsa-let-7i-5p (76, 89)
		hsa-miR-9-3p (78)

Table 2. Patient cohort characteristics.

		ENACT	PCBBR
		Median (Range)	
AGE (years)		62 (47-76)	62 (45-77)
PSA (ng/mL)		5.58 (0.47-14.17)	7.05 (3-735)
		N (%)	
RACE	**African American**	95 (67.4)	33 (53.2)
	Caucasian	25 (17.7)	15 (24.2)
	Hispanic	19 (13.5)	10 (16.1)
	Asian	2 (1.4)	0 (0)
	Multiple Races/Unknown	0 (0)	4 (6.5)
BIOPSY GLEASON GRADE GROUP	**1**	119 (84.4)	7 (11.3)
	2	22 (15.6)	34 (54.8)
	3	0 (0)	11 (17.7)
	4	0 (0)	7 (11.3)
	5	0 (0)	3 (4.8)
BIOPSY TO RP GLEASON GRADE COMPARISON*	**Upgraded**	10 (40.0)	17 (29.3)
	Downgraded	0 (0)	13 (22.4)
	Consistent	15 (60.0)	28 (48.3)
ADVERSE PATHOLOGY	**Yes**	8 (32.0)	36 (58.1)
	No	17 (68.0)	20 (32.2)
	Unknown	0 (0)	6 (9.7)

*Gleason Grade groups (GG) were compared at biopsy and at RP; patients with the same GG were qualified as “Consistent”, patients with higher GG at RP compared to biopsy were qualified as “Upgraded”, and patients with lower GG at RP compared to biopsy were qualified as “Downgraded”.